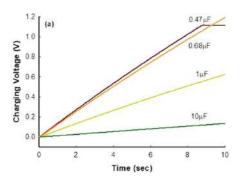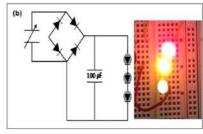Electrospun Polyvinylidene Fluoride-Polyoctafluoropentyl Acrylate-Hydroxyapatite Blend Based Piezoelectric Pressure Sensors

Ponnan Sathiyanathan,
Dhevagoti Manjula Dhevi,
Arun Anand Prabu*, and Kap Jin Kim**

Polyvinylidene fluoride (PVDF)-polyoctafluoropentyl acrylate (PFA) and hydroxyapatite (HAP) blend (PVDF-PFA/HAP) samples were electrospun under controlled conditions. Peak-to-peak output voltage of PVDF-PFA/HAP (93:7 w/w) blend sample exhibited significantly higher output voltage ($V_{p\text{-}p}$=1.21 V) and was utilized to charge different capacitors (0.47, 0.68, 1 and 10 µF) using bridge diode as a rectifier. Overall, the PVDF-PFA/HAP based nanoweb sensor can be used as a nanogenerator for charging LEDs and has great potential for many commercial sensor applications.

Electrospun Polyvinylidene Fluoride-Polyoctafluoropentyl Acrylate-Hydroxyapatite Blend Based Piezoelectric Pressure Sensors

Ponnan Sathiyanathan[1]
Dhevagoti Manjula Dhevi[2]
Arun Anand Prabu*,[3]
Kap Jin Kim**,[4]

[1] Department of Chemistry, Adhi College of Engineering and Technology, Sankarapuram, Kanchipuram, Tamil Nadu 631 605, India

[2] Department of Chemistry, SRM Institute of Science and Technology, Kattankulathur, Kanchipuram, Tamil Nadu 603 203, India

[3] Department of Chemistry, School of Advanced Sciences, Vellore Institute of Technology (VIT), Vellore, Tamil Nadu 632 014, India

[4] Department of Advanced Materials Engineering for Information and Electronics, College of Engineering, Kyung Hee University, Yongin-si, Gyeonggi-do 17104, Korea

Abstract: In this study, neat polyvinylidene fluoride (PVDF), PVDF/polyoctafluoro-pentyl acrylate (PFA, 90/10 w/w) and PVDF-PFA/hydroxyapatite (HAP, 0 to 20 wt.% HAP w.r.t. PVDF-PFA content) were electrospun under controlled conditions, and studied for their piezo-responsive behaviours as a function of nanoweb stacking arrangement (constructive and destructive) and folding architectures (simple, series and parallel connection of electrodes between each folding). Influence of varying HAP content (0, 3, 7, 10 and 20 wt.%) on the molecular orientation of CH_2-CF_2 dipoles in PVDF-PFA/HAP blends were investigated using FTIR, XRD and SEM analysis. Quantitative analysis showed increased β-crystalline content for the 7 wt.% HAP sample. From the peak-to-peak output voltage, 7 wt.% HAP sample exhibited significantly higher output voltage (V_{p-p}=1.21 V) compared to neat PVDF-PFA sample (V_{p-p}=0.46 V). Overall, the combinative effect of HAP addition and folding played a vital role in improving the piezoelectric output signals of PVDF-PFA/HAP, which signifies the importance of this study.

Keywords: PVDF, hydroxyapatite, electrospinning, pressure sensor, nanogenerator.

1. Introduction

Development of piezoelectric nanogenerator have been extensively studied as a reliable alternate renewable energy source in the form of micro electro-mechanical sensors for self-powered portable electronic devices.[1-10] Since the last decade, polyvinylidene fluoride (PVDF) and its copolymers based electrospun nanoweb sensors have attracted greater attention in electronic applications such as piezoelectric sensors,[3-5] heart-beat monitoring sensors[6] and in regenerative energy field as nanogenerator.[8,9] The suitable crystalline conformation for the fabrication of piezoelectric devices mostly depend on the β-crystalline phase content in PVDF based polymers. Various sample fabrication techniques such as solution- and spin-casting, electro-spinning, thermal treatment, poling under high electric field, uni- or bi-directional drawing of films were employed to achieve favorable chain-dipole orientation in PVDF and its copolymers resulting in higher β-crystalline phase.[11-13] Using electrospun PVDF nanofiber web, Lee *et al.* measured the electrical activity of human body generated electrocardiogram (ECG).[6] In an earlier report,

we investigated the physico-mechanical and piezo-responsive behaviors of electrospun neat PVDF and its blend with polyoctafluoropentyl acrylate (PFA, 10 wt.% w.r.t. PVDF), herein referred to as PVDF-PFA (90/10) blend.[14] Though the peak-to-peak piezoelectric output signal obtained for PVDF-PFA (90/10) blend sample (V_{p-p}=0.46 V) was lower than neat PVDF (V_{p-p}=1.195), the blend sample exhibited higher piezo-capacitance hysteresis (C_{max}=0.182 nF) and enhanced elasticity in nanoweb (65.2±0.4 kPa) compared to neat PVDF (C_{max}=0.147 nF, 1.5±0.03 kPa). In recent years, many researchers have also studied the effect of metal nanoparticles and metal salts on the β-crystalline content in PVDF.[15-18] In the case of metals salts, our research group has investigated the α- and β-crystalline phase changes in as-cast PVDF thick films as a function of varying mass fractions (0 to 20 wt.%) of calcium chloride ($CaCl_2$) salt.[16] PVDF-$CaCl_2$ (15 wt.%) sample exhibited higher β-crystalline content along with a remnant polarization of 3.1 $\mu C/cm^2$. In our recent study, PVDF-$CaCl_2$ sample exhibited relatively higher peak-to-peak output voltage (V_{p-p}=+0.89 V) than neat PVDF (V_{p-p}=+0.48 V).[18] Jana *et al.* fabricated high performance piezoelectric energy harvesters using PVDF-$MgCl_2$ and generated sufficient power to turn on commercial LEDs.[17] Aforementioned literatures served as an evidence for the possibility of using PVDF based electrospun nanoweb sensors as piezoelectric nanogenerator in power generation for portable devices and for monitoring vital signals on the human body.
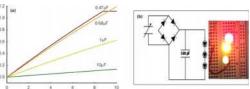
*Corresponding Author: Arun Anand Prabu (anandprabu@vit.ac.in)
Kap Jin Kim (kjkim@khu.ac.kr)

Hydroxyapatite (HAP) has generated greater interest among researchers as a common biomaterial used in biomedical fields such as dental implant, orthopedic, tissue engineering, drug delivery, etc. due to its excellent biocompatibility and mechanical strength.[19,20] Similar to PVDF, HAP also shows a reversible polarization and ferroelectric behavior with significant higher piezoelectric coefficient (16 pC.N^{-1}) and pyroelectric coefficient (12 μC.m^{-2}.K^{-1}). In earlier studies, Lang *et al* investigated the crystallinity and mechanical strength of PVDF/HAP based membranes.[19] Compared to neat HAP, the melting temperature and crystallinity of PVDF/HAP membrane was found to be increasing with that of HAP concentration in PVDF. Young's modulus of PVDF-HAP also increased from 66.76 MPa to 129.9 MPa with increasing HAP content from 0 to 3 wt.%. Tensile strength of PVDF/HAP also improved from 2.54 (1 wt.% HAP) to 4.31 MPa (3 wt.% HAP). Moreover, elongation at break also improved with the addition of HAP in PVDF. These results are evidence towards increasing crystallinity and mechanical strength of PVDF with the addition of HAP.

In the present report, we chose to study the effect of HAP content on the piezoelectric behavior of PVDF-PFA based electrospun nanoweb sensors. Based on the optimized conditions, PVDF-PFA/HAP nanoweb sensor with constructive stacking and parallel folding of top/bottom electrode was used as a nanogenerator to power up LEDs and as a physiological sensor to measure vital signals on human body. Comparative studies on neat PVDF and PVDF-PFA/HAP silver-plated nanoweb sensors for measuring electrocardiogram (ECG) were also performed. The results are discussed in detail.

2. Experimental

2.1. Materials and methods

PVDF (Kynar® 761, M_w=370,000) and 2,2,3,3,4,4,5,5-octafluoropentyl acrylate (OFA) monomer were purchased from Samchun (Korea) and Atochem® (USA), respectively. OFA was polymerized using reported procedure[21] and herein mentioned as PFA. Hydroxyapatite (HAP) nanoparticles were synthesized from chicken bone using a procedure given elsewhere.[22] Isolation and confirmation of HAP particles formation are given in Supporting Information (Figures S1 to S3 and Table S1). PVDF-PFA (90/10) blend (herein mentioned as PVDF-PFA) and PVDF-PFA/HAP blends (0, 3, 5, 7, 10, 20 wt.% of HAP w.r.t PVDF-PFA) were dissolved in DMF: acetone solvent mixture (6:4 v/v) to prepare 2 wt.% solution (w/v, for as-cast film) and 18 wt.% solution (w/v, for electrospinning). The purpose of adding acetone is to assist in the faster evaporation of the DMF solvent during as-cast/electrospinning at ambient temperature condition. The maximum amount of PFA in PVDF is restricted to 10 wt.% beyond which it exhibit coagulation effect and blocking of the needle during electrospinning. Electrospinning parameters used to prepare the nanoweb are given in Supporting Information (Table S2).
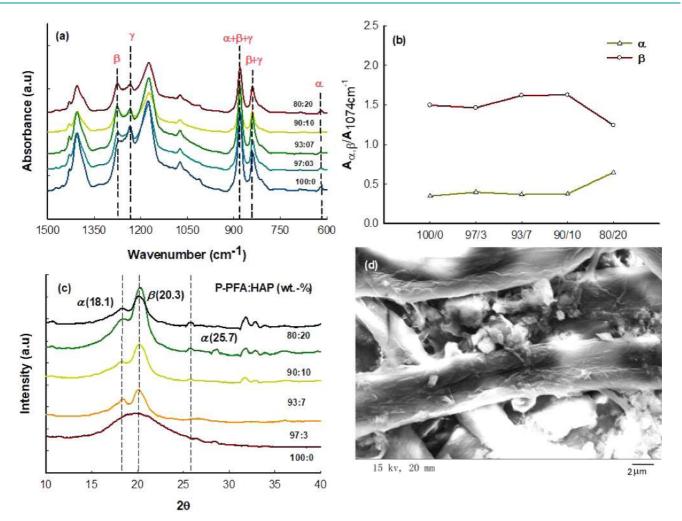
2.2. Characterization

FTIR-TS were collected using Bruker-IFS66V spectrometer with 100 scans at a resolution of 4 cm^{-1}. Morphology of the samples was observed using scanning electron microscope (SEM, ZEISS ULTRA 55, 20 kV, Germany). Powder X-ray diffraction was analyzed using Bruker (Model-D8 Advance; Germany) X-ray diffractometer - Cu Kα radiation 1 in the 2θ range 10-80°. Sensor fabrication, testing set-up and the simplified equivalent circuit model used for measuring the piezoresponsive signals are given in Supporting Information as Figures S4 to S6, respectively. In brief, the piezoelectric output signals (V/mg) were generated by applying 1 kgf of sinusoidal pressure with 0.5 Hz on the sensor using a custom-made dynamic pressure instrument and the signals were transferred to the preamplifier (Piezo Film Lab Amplifier, Measurement Specialties Inc., USA) as a function of varying sensor architecture, viz. (i) constructive and destructive stacking, and (ii) simple folding, folding with series connection of electrode and folding with parallel connection of electrodes.
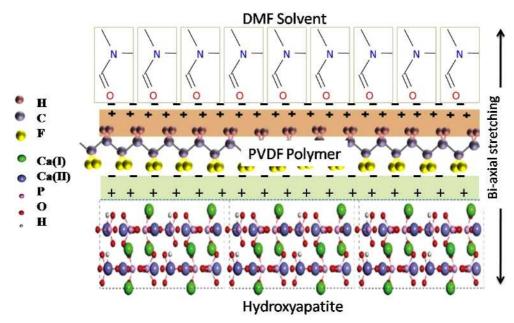
3. Results and discussion

3.1. FTIR, XRD and SEM analyses

From the previous reports, PVDF exhibit characteristic FTIR absorption bands at 486, 532, 613, 763, 796 and 976 cm^{-1} corresponding to α-crystalline phase, 509, 840 and 1279 cm^{-1} corresponding to β-crystalline phase and 1232 cm^{-1} band for γ-crystalline phase.[16,23,24] Figure 1(a) shows the FTIR spectral data of PVDF-PFA/HAP thick film samples as a function of varying weight percentage of HAP (0, 3, 7, 10, 20 wt.%). As-cast samples of neat PVDF generally shows α-phase at room temperature, which upon adding nanoparticles or subjected to thermal treatment, exhibit crystalline transformation from α-crystalline phase to β-crystalline phase.[12,16] In our previous work,[14] we reported higher β-crystalline content for PVDF-PFA (90/10) blend as-cast sample annealed at ambient temperature (30 °C), and with increasing annealing temperature (60~150 °C), the β-crystalline content decreased drastically. In the present study, relative increase in β-phase with increasing HAP content was observed for the as-cast PVDF-PFA/HAP samples but shows a decreasing trend at higher concentrations above 10 wt.%. Quantitative FTIR data (Figure 1(b) showed higher β-crystalline content for 7 wt.% HAP sample. X-ray diffraction pattern (Figure 1(c)) supports the FTIR data in which the same trend was observed on β-phase (110) corresponding to 2θ=20.3. On the other hand, the peaks at 2θ=18.1 and 25.7 corresponding to α-phase (100) and (021)[11] showed decreasing trend as the HAP content increased beyond 10 wt.%. The effect of adding HAP in PVDF-PFA as-cast samples resulted in crystalline phase transformation from α- to β-crystalline phase and it is very clear that the C-F dipoles in β-crystalline phase is oriented (net dipole moment > 0) upon the addition of HAP in PVDF-PFA. From FTIR and XRD data, the observed α- to β-crystalline phase transformation in PVDF-PFA/HAP samples is effectively confirmed. Further, a mechanism is proposed (Scheme 1) depicting the hydrogen bonding interaction between OH in HAP, CH$_2$-CF$_2$ dipoles in PVDF and O=C-N in DMF as O-H···F-CF-CH-H···O=C-N.[25,26] This interaction could influence the reorientation of CH$_2$-CF$_2$ dipoles in PVDF from *trans-gauche* (TGTG') to *all-trans* (TTTT) conformation, thereby result-

Figure 1. (a) FTIR spectra of PVDF-PFA/HAP thick films subjected to different weight percentage of HAP (b) FTIR quantitative data extracted from Figure 1(a) as a function of α-, β- and γ-crystalline peak absorbance ratios; (c) XRD pattern of PVDF-PFA/HAP thick films; (d) FE-SEM image of electrospun PVDF-PFA/HAP nanofiber web at 20.0 KX magnifications.

Scheme 1. Mechanism of hydrogen-bonding interaction between PVDF, HAP and DMF solvent.

ing in higher β-crystalline phase in PVDF.

Figure 1(d) shows the SEM morphology of PVDF-PFA/HAP

(93:7) electrospun nanoweb sample. Unlike non-linear *root-shaped* nanofiber[14] observed in the case of neat PVDF-PFA, a uniform

morphology is observed in PVDF-PFA/HAP sample along with the clear observation of HAP nanoparticles. SEM image measured for PVDF-PFA sample exhibited non-linear *root-shaped* network which made nanofiber highly elastic in nature. This might have arisen from restrictive stretching of PVDF-PFA samples during electrospinning process and the poor solvent-polymer interaction. In our earlier study, we reported the preferential orientation of C-F dipoles (leading to higher *β*-crystalline phase) in PVDF dissolved in DMF: acetone (60:40) solvent mixture, and this behavior is attributed to the polymer-solvent interaction (C-H⋯O=C-N) and faster evaporation of the low-boiling acetone solvent.[24] Compared to that, the P-PFA/HAP nanofiber obtained in the present work exhibit a clear fiber formation similar to neat PVDF. Based on the FTIR, XRD and SEM data, further studies were focused on the piezoelectric measurements of selected PVDF-PFA/HAP nanoweb samples using different stacking and folding architectures, which could confirm the suitability of using this blend material as a piezoelectric nanogenerator (oriented, net dipole moment > 0) in energy harvesting and physiological sensor applications.

3.2. Piezoelectric measurements

It is well-known that electrospun PVDF nanoweb samples exhibits higher *β*-crystalline phase than as-cast or solution-cast samples.[14] The combined effect of *in-situ* poling (high voltage supply of ~18 kV) and internal stretching employed during the electrospinning result in the re-orientation of polymeric chains which in turn induce significantly higher ferroelectric and piezoelectric properties in nanofiber.[25] Figure 2(a) and (b) shows the comparative piezoelectric output signals of PVDF-PFA/HAP electrospun nanoweb samples for varying HAP concentration (0, 3, 7, 10 and 20 wt.% of HAP). V_{p-p} for neat PVDF-PFA sample showed lesser value (0.46 V) compared to PVDF-PFA/HAP samples and it tends to increase with increasing content of HAP till 7 wt.% (1.21 V). Beyond this HAP content, V_{p-p} values showed a decreasing trend. The addition of 3 and 7 wt.% HAP improved the interaction between polymer and HAP, but increasing addition of HAP content above 7 wt.% tends to show decreased V_{p-p} value (10 wt.%=0.89 V and 20 wt.%=0.40 V). This trend is attributed to higher HAP content causing coagulation and solvent miscibility during electrospinning process which hinders the fiber orientation resulting in the formation of unfavorable *trans-gauche* (TGTG') crystalline phase. Figure 2(c) and (d) compares the piezoelectric output voltage as a function of different stacking arrangement of nanoweb to distinguish the orientation of C-F dipoles between the constructive and destructive stacking. In our previous report, the neat PVDF-PFA sample showed similar value both in constructive (PVDF-PFA-C; V_{p-p}=0.67 V) and destructive (PVDF-PFA-D; V_{p-p}=0.67 V) stacking which prove that the C-F dipoles are randomly oriented irrespective of stacking arrangement.[14,25] As shown in Figure 2(c) and (d), PVDF-PFA/HAP-Constructive stacking exhibited higher V_{p-p}=1.28 V than PVDF-PFA/HAP-Destructive stacking (V_{p-p}=0.6 V). This data serves as evidence that PVDF-PFA/HAP nanoweb sensor can be effectively used as a 'nanogenerator' in microelectronic applications.

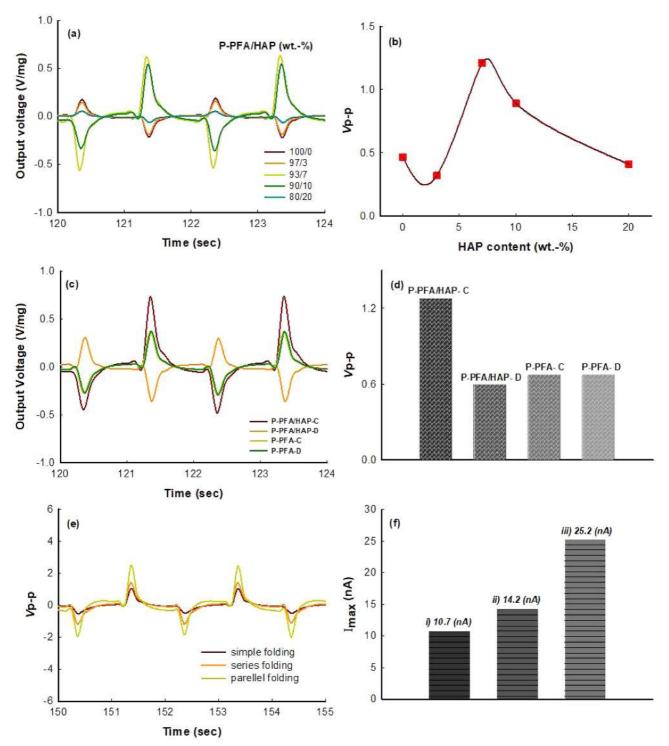Further studies were carried out using folded nanofiber web between top and bottom electrodes by three different methods: viz. (a) simple folding, (b) folding with series connection of electrodes, and (c) folding with parallel connection of electrodes.[27,28] Among these three folding types, folding with parallel connection of electrodes showed significantly greater V_{p-p} value due to the improved conductivity in between the pair of each layers through inserting parallel-connected electrodes. On the other hand, simple and series folding showed reduced V_{p-p} value and this may be attributed to the insulating effect of air trapped between the folded nanoweb layer and the lack of direct electrical contact between the nanoweb layers in simple and series folding.[27] As shown in Figure 2(e) and (f), the maximum output current (I_{max}) derived from the mathematical relationship I_{max} (A)=V_{max}(V)/R_{in}(Ω) obtained through these three folding, parallel connection showed higher value (I_{max}=25.2 nA, V_{p-p}=2.52 V) than series folding (I_{max}=14.2 nA, V_{p-p}=1.42 V) and simple folding (I_{max}=10.7 nA, V_{p-p}=1.07 V). Irrespective of the nanoweb layers used in different folding, the paths for the current flows between the top and bottom electrode define the power output. In the case of simple folding, the current flows through only one pathway between top and bottom electrodes, whereas in parallel folding, the current flows through multiple pathways as the area of active piezoelectric material is effectively multiplied with the number of layers used without increasing the distance between them.

3.3. Capacitor charging and LED operation

From the above results, it is evident that the parallel folding of PVDF-PFA/HAP nanoweb sensor showed enhanced output voltage and can be used as a power source for charging capacitor and operating LEDs. Earlier, Lee et al demonstrated the possibility of using parallel folding of PLA based nanoweb sensor as a power source.[27] In the present work, PVDF-PFA/HAP (93:7) nanoweb sensor with 9 layered stacking of parallel-connected electrodes with diameter of active material area about 2 to 3 cm was fabricated in order to increase the efficiency of charging voltage. The output voltage derived from sensor was used to charging different capacitors (0.47, 0.68, 1 and 10 μF) using bridge diode as a rectifier (Figure 3(a)). When the charging voltage approaches the LED driving voltage as a function of time, LEDs were turned 'ON' (Figure 3(b)). Initially, thin capacitor with the capacity value of 0.47 μF was charged and it is observed that smaller capacitors charged quickly within a shorter time (8 to 100 seconds), whereas thicker capacitor (10 μF) takes more time (2000 seconds) to charge completely. On the other hand, the discharging of current was quicker when LEDs are attached with smaller capacitor resulting in faster blinking of LEDs. When 10 μF capacitor was used, the discharging behavior of thicker capacitor is less due to the fact that the consumption of current taken by LEDs are quite smaller than charge stored on the capacitor.
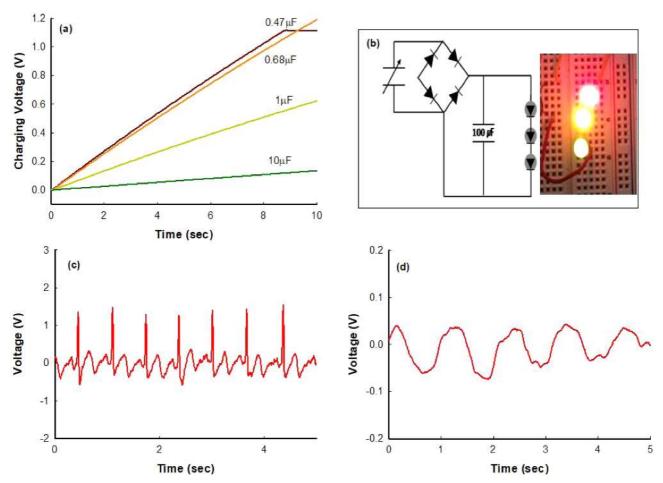
3.4. ECG and respiration signals

ECG measures the electrical activity from our heartbeat that is generated during contraction and release of a myocardium.[6] Lee *et al.* studied the pyroelectric and shear-piezoelectric behaviors of polylactic acid nanoweb sensors embedded close

Figure 2. Piezoelectric output voltage of PVDF-PFA measured at varying weight percentage of HAP: (a) as a function of single layer and (b) their $V_{p\text{-}p}$ data; (c) as function of constructive (C) and destructive (D) stacking architectures and (d) their $V_{p\text{-}p}$ data; (e) as a function of different folding: (i) simple folding, (ii) folding with series connection of electrodes (R_{in}=1 GΩ, Gain=0 dB), (iii) folding with parallel connection of electrode (R_{in}=100 MΩ, Gain=0 dB); and (f) current (I_{max} (A)=V_{max} (V)/R_{in}(Ω) comparison plot.

to human body and measured the piezo and pyroelectric sensor signals originated from changes in deformation action of body movement and body temperature, respectively.[27] In the present study, the monitoring of human heart beat signals by electrocardiogram (ECG) analysis using non-conventional dry-type electrodes compared to conventional gel-type electrode (Ag/AgCl) was attempted. Fabrication of electroless silver plat-ing of PVDF-PFA/HAP (93:7) nanoweb sensor used as a dry-type electrode for ECG measurement and the detailed fabrication process are given elsewhere.[28] Compared to PVDF-PFA nanoweb sensor, the ECG signals obtained from PVDF-PFA/HAP (93:7) ECG sensor showed significant higher value with an average period of about 0.783 sec between each signal and the heart beat rate is estimated to be 76 beats per minute (Figure 3(c)).

Figure 3. (a) Charging voltage vs. time for capacitors having different capacitances; (b) equivalent circuit diagram to operate LED diodes and photograph of LEDs operated using a 100 mF capacitor when connected, (c) ECG signals obtained using electroless silver-plated PVDF-PFA/HAP nanoweb sensor; (d) respiration signals obtained from PSB tied around the chest at rest.

Respiratory signals were measured using plethysmography belt wrapped around chest or abdomen of the human body. The circumference changes of the chest or the abdomen could be analyzed by this technique which is an important application in monitoring vital signals in human body.[29,30] Fabrication of PSB belt was done by embedding the silicon rubber/carbon black/conductive carbon layer coated PVDF-PFA/HAP nanoweb in elastic textile bands as per the procedure given elsewhere.[6,29] Changes in the C-F dipole orientation of PVDF-PFA/HAP nanoweb was found to generate significant current (V_{p-p}=1.03 V) aided by the elongating nanoweb across the chest during respiration process (Figure 3(d)).

4. Conclusions

In this study, the crystalline phase changes of PVDF-PFA/HAP samples were studied as a function of different weight percentage of HAP (0 to 20 wt.%) using FTIR, XRD and SEM analysis. Piezoelectric behaviors were analyzed through different arrangement of stacking and folding the nanoweb sensors. Finally, the selected nanoweb sensors were demonstrated for heart-beat monitoring (ECG) and respiration monitoring in health care. The results are summarized as follows:

(1) The relative increase in β-crystalline phase with increasing weight percentage of HAP was observed for the as-cast PVDF-PFA/HAP samples but showed a decreasing trend at concentrations above 10 wt.%. Among the varying HAP content, the samples with 7 wt.% of HAP showed higher β-crystalline phase compared to neat PVDF-PFA.

(2) Peak-to-peak output voltage (V_{p-p}) measured for PVDF-PFA/HAP (93:7) sample showed maximum value (V_{p-p}=1.21 V) and it is clearly observed that with increasing HAP content until 7 wt.%, V_{p-p} value also increased. Similarly, the studies carried out using constructive and destructive stacking arrangement of HAP added nanoweb confirmed reorientation of C-F dipoles (favorable β-crystalline phase) in PVDF-PFA/HAP, thereby resulting in higher V_{p-p} value (1.28 V) for constructive stacking (PVDF-PFA/HAP-C).

(3) Among the different folding, nanoweb sensor with parallel folding exhibited enhanced piezoelectric signals (I_{max}=25.2 nA) and used as a power source to operate LEDs.

(4) ECG for monitoring human heart-beat signals using dry-type silver-plated PVDF-PFA/HAP conductive nanoweb sensor showed promising results. Additionally, the PSB sensor fabricated in this study is successfully used to monitor respiratory behavior of human body.

(5) Overall, the nanoweb sensors used as a nanogenerator for charging the LEDs and for monitoring human heart-beat signals

indicate the great potential of PVDF-PFA/HAP blend material for many commercial sensor applications.

Supporting Information: Information is available regarding the isolation of hydroxyapatite particles and its characterization, electrospinning parameters for the preparation of nanoweb, piezoelectric sensor model, measuring setup, and equivalent circuit diagram. The materials are available *via* the Internet at http://www.springer.com/13233.

References

(1) G. H. Kim, *Macromol. Res.*, **12**, 564 (2004).

(2) J. S. Lee, A. A. Prabu, and K. J. Kim, *Polymer*, **51**, 6319 (2010).

(3) Y. R. Wang, J. M. Zheng, G. Y. Ren, P. H. Zhang, and C. Xu, *Smart Mater. Struct.,* **20**, 045009 (2011).

(4) B. Zhang, L. M. Lei, J. Yang, X. H. Guo, and G. P. Zhang, *Mater. Lett.,* **89**, 302 (2012).

(5) S. H. Kim, A. Leung, C. Y. Koo, L. Kuhn, W. Jiang, and D. J. Kim, *Mater. Lett.,* **69**, 24 (2012).

(6) S. Lee, Y. Ahn, A. A. Prabu, and K. J. Kim, *J. Fiber Bioeng. Inform.,* **6**, 369 (2013).

(7) C. R. Bowen, H. A. Kim, P. M. Weaver, and S. Dunn, *Energy Environ. Sci.*, **7**, 25 (2014).

(8) A. Tamang, S. K. Ghosh, S. Garain, M. M. Alam, J. Haeberle, K. Henkel, D. Schmeisser, and D. Mandal, *Appl. Mater. Interfaces*, **7**, 16143 (2015).

(9) S. K. Ghosh and D. Mandal, *Appl. Phys. Lett.*, **109**, 103701 (2016).

(10) Y. Gao, M. Wei, X. Li, W. Xu, A. Ahiabu, J. Perdiz, Z. Liu, and M. J. Serpe, *Macromol. Res.*, **25**, 513 (2017).

(11) Y. J. Park, Y. S. Kang, and C. Park, *Eur. Polym. J.*, **41**, 1002 (2005).

(12) S. J. Kang, Y. J. Park, I. Bae, K. J. Kim, H. C. Kim, S. Bauer, E. L. Thomas, and C. Park, *Adv. Funct. Mater.*, **19**, 2812 (2009).

(13) D. Mandal, S. Yoon, and K. J. Kim, *Macromol. Rapid Commun.,* **32**, 831 (2011).

(14) P. Sathiyanathan, A. A. Prabu, and K. J. Kim, *Macromol. Res.*, **24**, 670 (2016).

(15) T. R. Hebner, C. C. Wu, D. Marcy, M. H. Lu, and J. C. Sturm, *Appl. Phys. Lett.*, **72**, 519 (1998).

(16) S. Yoon, A. A. Prabu, K. J. Kim, and C. Park, *Macromol. Rapid Commun.,* **29**, 1316 (2008).

(17) S. Jana, S. Garain, S. Sen, and D. Mandal, *Phys. Chem. Chem. Phys.*, **17**, 17429 (2015).

(18) G. Prasad, P. Sathiyanathan, A. A. Prabu, and K. J. Kim, Macromol. Res., 25, 981 (2017).

(19) S. B. Lang, S. A. M. Tofail, A. A. Gandhi, M. Gregor, C. Wolf-Brandstetter, J. Kost, S. Baue and M. Krause, *Appl. Phys. Lett.*, **98**, 123703 (2011).

(20) S. B. Lang, S. A. M. Tofali, A. L. Kholkin, M. Wojtas, M. Gregor, A. A. Gandhi, Y. Wang, S. Bauer, M. Krause and A. Plecenik, *Scientific Reports,* **3**, 2215 (2013).

(21) N. A. Storozhakova, V. A. Korotkikh, A. I. Rakhimov, and T. I. Danilenko, *J. App. Polym. Sci.*, **101**, 4028 (2006).

(22) R. Rajesh, A. Hariharasubramanian and Y. D. Ravichandran, *Phosphorus, Sulfur Silicon Relat. Elem.,* **187**, 914 (2012).

(23) D. M. Dhevi, A. A. Prabu, M. Pathak, and K. J. Kim, *Adv. Mater. Res.*, **584**, 197 (2012).

(24) D. M. Dhevi, A. A. Prabu, and M. Pathak, *Polymer*, **55**, 886 (2014).

(25) W. Ma, J. Zhang, and X. Wang, *J. Mater. Sci.,* **43**, 398 (2008).

(26) W. Ma, J. Zhang, S. Chen, and X. Wang, *J. Macromol. Sci.*, **47**, 434 (2008).

(27) S. J. Lee, A. A. Prabu, and K. J. Kim, *Mater. Lett.*, **148**, 58 (2015).

(28) Y. J. Ahn, S. Yoon, K. J. Kim, *Text. Sci. Eng.*, **49**, 47 (2012).

(29) A. M. Sinton, and R. Suntheralingam, *Med. Biol. Eng. Comput.*, **26**, 213 (1988).

(30) Y. M. Chang, J. S. Lee, and K. J. Kim, *Solid State Phenom.,* **124**, 299 (2007).

Supporting Information

1. Isolation of hydroxyapatite (HAP) from chicken bone

Natural bone consists of around 70% inorganics, 20% organics and 10% water. Organic component is mostly made of type-I collagen and inorganic mineral consists of carbonated hydroxyapatite. In this work, HAP was isolated from chicken bones by thermal-calcination method. At first, bone samples were washed with water and then soaked in saturated NaOH overnight to remove traces of meat and skin. After drying at 100 $^{\circ}$C, the samples were grounded into finer pieces and calcined at 800 $^{\circ}$C for 16 h in an electric furnace.

2. Characterization of HAP particles

FT-IR, XRD and SEM morphology of HAP are shown in Figures S1 to S3, respectively. HAP sample calcined at 800 $^{\circ}$C does not showed any characteristic band (amide-I band of the collagen: organic matter) at 1650 cm^{-1} due to complete removal of organic matrix present in the chicken bone. Further, appearance of an additional peak at 962 cm^{-1} (ν_sPO$_4^{3-}$) in the bones calcined above 800 $^{\circ}$C indicates the presence of HAP free from organic matter. Table S1 shows the characteristic bands observed in HAP calcined at 800 $^{\circ}$C which confirms the formation of HAP particles.
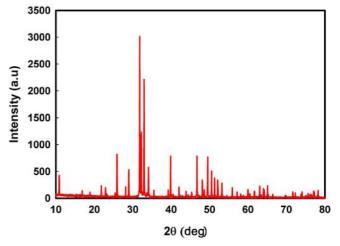

Figure S2. XRD pattern for HAP calcinated at 800 $^{\circ}$C.

XRD pattern for HAP calcinated at 800 $^{\circ}$C was found to be in good conformity with the standard values of HAP (JCPDS-09-0432=1996) along with the three characteristic peaks appearing at 31.75°, 32.15° and 32.90°. Further, SEM morphology of HAP exhibited crystalline rod-like structure in the isolated HAP particles.
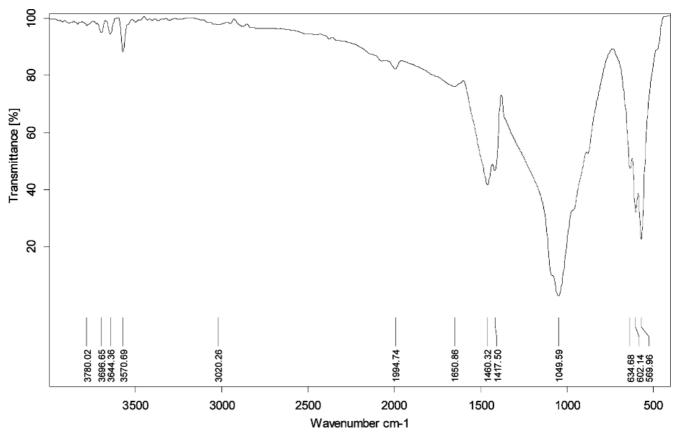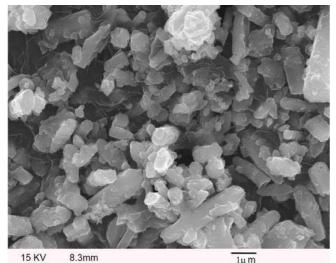

Figure S1. FT-IR spectrum of HAP calcinated at 800 $^{\circ}$C.

Figure S3. FE-SEM image of HAP particles calcinated at 800 °C.

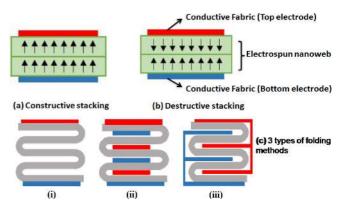**Table S1.** Characteristic bands observed in HAP sample calcined at 800 °C

Wavenumber (cm⁻¹)	Assignments
1092-1049	Symmetrical triply degenerate O-P-O bending (ν_s PO$_4^{3-}$)
962	Symmetrical nondegenerate P-O stretching (ν_s PO$_4^{3-}$)
570-569	Triply degenerate antisymmetric and harmonic O-P-O bending (ν_{as} PO$_4^{3-}$)
603-601	Antisymmetric doubly degenerate P-O stretching (ν_{as} PO$_4^{3-}$)

Table S2. Electrospinning parameters used for preparing nanoweb

Weight % of solution	18 wt.%
Injection Volume	6 mL
Injection Rate	1.2 mL/h
Tip-collector drum distance(TCD)	15 cm
Needle size	23G
Applied voltage	11.5-12 KV
Collector rotating rate	60 rpm
Humidity	50-60%
Temperature	20-25 °C

3. Electrospinning parameters and sensor fabrication methods

Table S2 shows the electrospinning parameters used for preparing nanoweb. Different types of sensor architecture were fabricated using a nickel-copper plated conductive fabrics of 2 cm diameter (J. G. Korea Inc., Korea) adhered to each side of the nanofiber web as top and bottom electrodes, and further encapsulated using adhesive transparent tape for protection (Figure S4). The piezoelectric output signals (V/mg) were generated using a custom-made dynamic pressure instrument and the signals were transferred to the preamplifier (Piezo Film Lab Amplifier, Measurement Specialties Inc., USA) (Figures S5 and S6).

Figure S4. Different piezoelectric sensor model: (a) constructive stacking and (b) destructive stacking; (c) 3 types of nanoweb folding used in this study: (i) simple folding, (ii) folding with series connection of electrode, and (iii) folding with parallel connection of electrode.
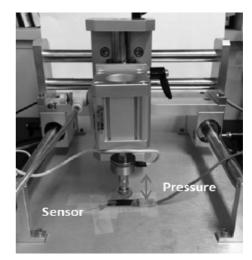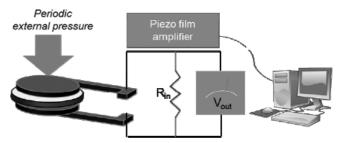

Figure S5. Dynamic pressure measuring custom-made setup.

Figure S6. Equivalent circuit diagram for measuring piezoelectric output signal.